Electronic Supporting Information

Intracellular detection of Cu^{2+} and S^{2-} ions through a quinazoline functionalized benzimidazole-based new fluorogenic differential chemosensor

Anup Paul,[a]* Sellamuthu Anbu,[a] Gunjan Sharma,[b] Maxim L. Kuznetsov,[a] Fátima C. Guedes da Silva,[a] Biplob Koch,[b] Armando J. L. Pombeiro[a]*

[a]*Centro de Química Estrutural, Complexo I, Instituto Superior Técnico,Universidade de Lisboa, Av. Rovisco Pais, 1049-001 Lisboa. Portugal. E-mail: kanupual@gmail.com, pombeiro@tecnico.ulisboa.pt*

[b]*Department of Zoology, Faculty of Science, Banaras Hindu University, Varanasi - 221 005 (U.P.) India.*

Contents:

1. **Fig. S1**, ^1H spectrum of $\mathbf{H_3L}$ S2
2. **Fig. S2**, ^{13}C NMR spectrum of $\mathbf{H_3L}$ S2
3. **Fig. S3**, ESI-MS spectrum of $\mathbf{H_3L}$ S3
4. **Fig. S4**, ESI-MS spectrum of $\mathbf{H_2L\text{-}Cu^{2+}}$ in CH_3OH S3
5. **Fig. S5.** Experimental and simulated of isotopic distribution of $\mathbf{H_2L\text{-}Cu^{2+}}$ at m/z = 467.76. S4
6. **Fig. S6**, Spin density distribution in complex $[Cu(HR)(H_2O)]H_2O$ (**d**) S4
7. **Fig. S7**, pH effect on the fluorescence intensity of $\mathbf{H_3L}$ and $\mathbf{H_2L\text{-}Cu^{2+}}$ S5
8. **Fig. S8**, UV-vis spectra of $\mathbf{H_3L}$ and $\mathbf{H_2L\text{-}Cu^{2+}}$ S5
9. **Fig. S9**, Naked eye and fluorescence changes of $\mathbf{H_3L}$ with Cu^{2+} and CN^- S6
10. **Fig. S10**, Job's plot for $\mathbf{H_3L}$ and Cu^{2+} from absorption data S6
11. **Fig. S11**, Time dependent fluorescence response of $\mathbf{H_3L}$ with Cu^{2+} S7
12. **Fig. S12**, Job's plot for $\mathbf{H_3L}$ with Cu^{2+} from emission data S7
13. **Fig. S13**, Detection limit for Cu^{2+} S8
14. **Fig. S14**, Interference of other anions in presence of $\mathbf{H_2L\text{-}Cu^{2+}}$ S8
15. **Fig. S15** Change in the absorption intensity of $\mathbf{H_2L\text{-}Cu^{2+}}$ upon addition of CN^- S9
16. **Fig. S16** Change in the fluorescence intensity of $\mathbf{H_2L\text{-}Cu^{2+}}$ upon addition of CN^- S9

17. **Fig. S17**, Detection limit for S^{2-} S10

18. **Fig. S18**, Time dependent fluorescence response of $\mathbf{H_2L\text{-}Cu^{2+}}$ for $\mathbf{CN^-}$ S10

19. **Fig. S19** ESI-MS spectrum of $\mathbf{H_2L\text{-}Cu^{2+}}$ in presence of Na_2S S11

20. **Fig. S20**, MTT assay for $\mathbf{H_3L}$ and $\mathbf{H_2L\text{-}Cu^{2+}}$ on DL cells S11

References

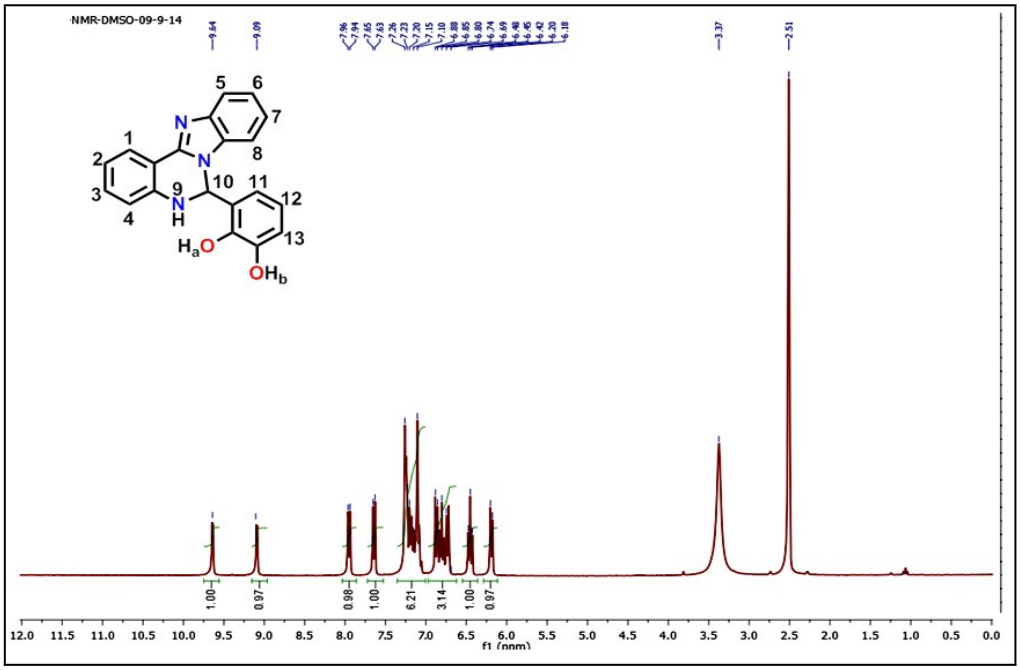

Fig. S1. ^{1}H NMR NMR spectrum of $\mathbf{H_3L}$ recorded in DMSO-d_6.

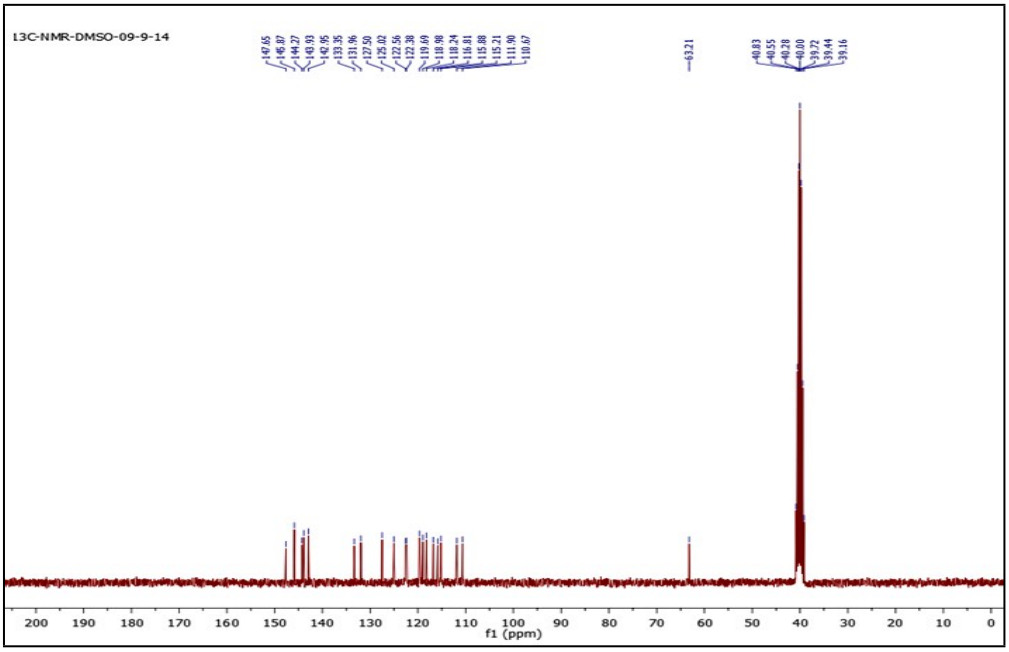

Fig. S2. ^{13}C NMR spectrum of $\mathbf{H_3L}$ recorded in DMSO-d_6.

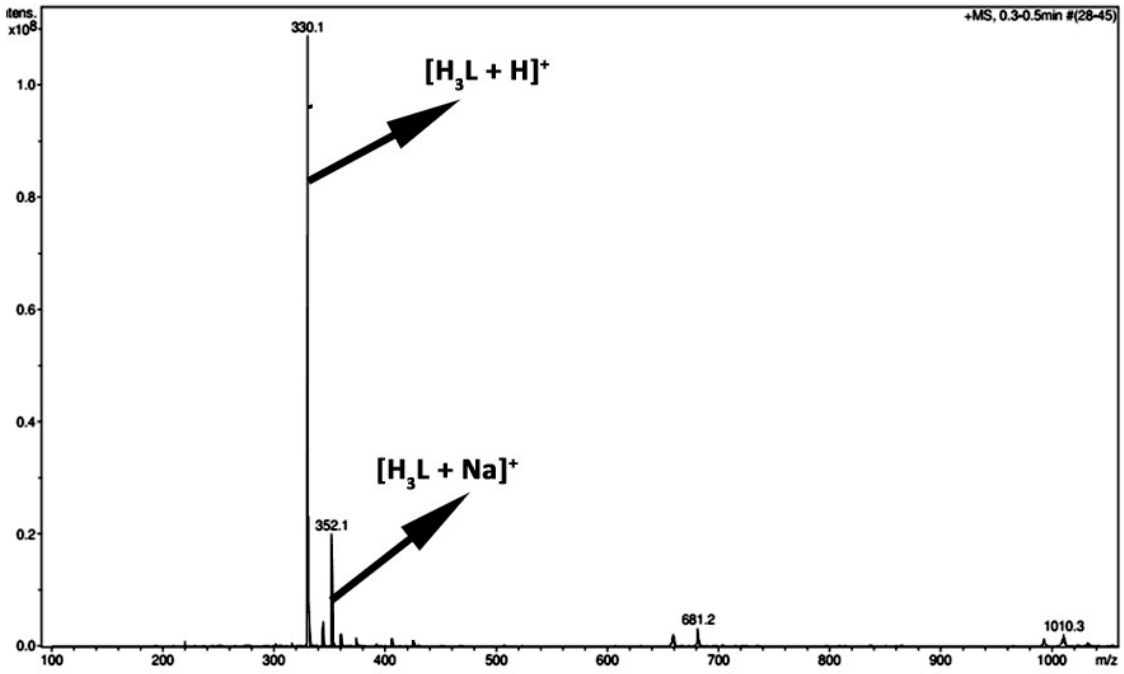

Fig. S3. ESI-MS spectrum of $\mathbf{H_3L}$ in CH_3OH.

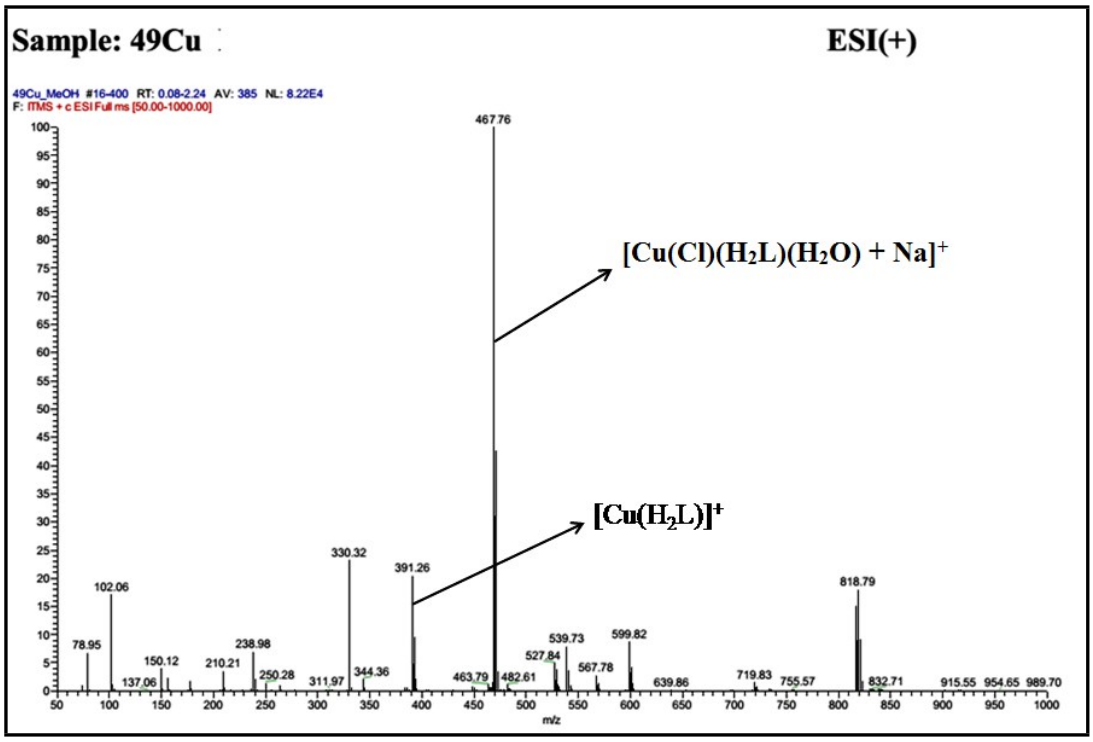

Fig. S4. ESI-MS spectrum of $\mathbf{H_2L\text{-}Cu^{2+}}$ in CH_3OH.

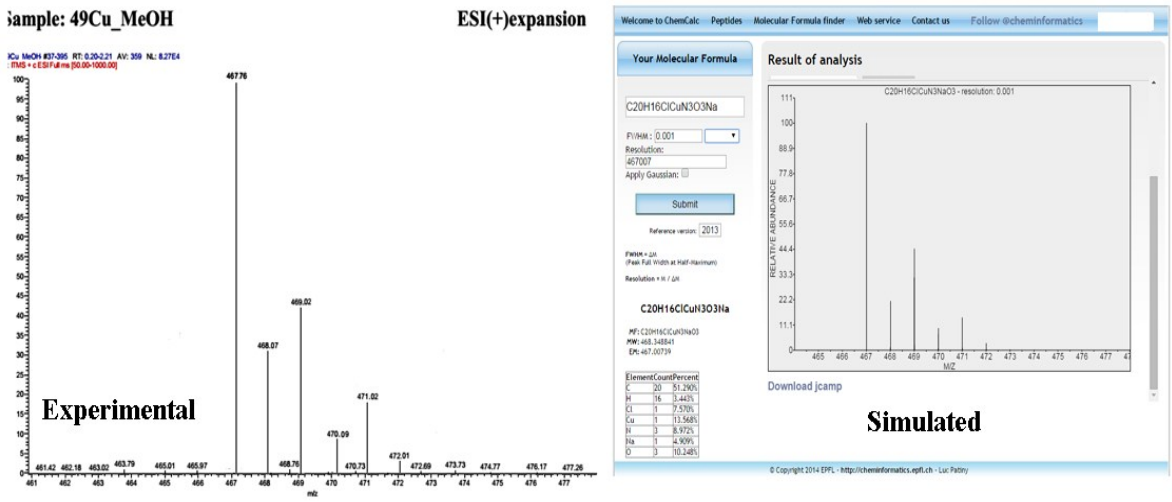

Fig. S5. Experimental and simulated[1] of isotopic distribution of $[Cu(Cl)(H_2L)(H_2O) + Na]^+$ at m/z = 467.76.

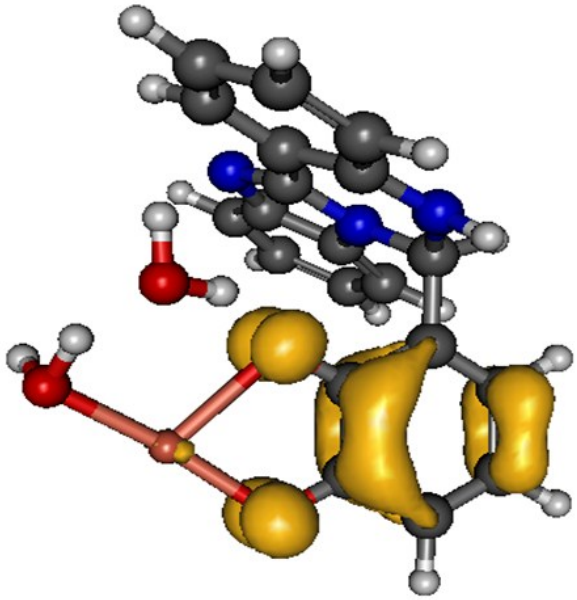

Fig. S6. Spin density distribution in complex $[Cu(HL)(H_2O)]H_2O$ (**d**).

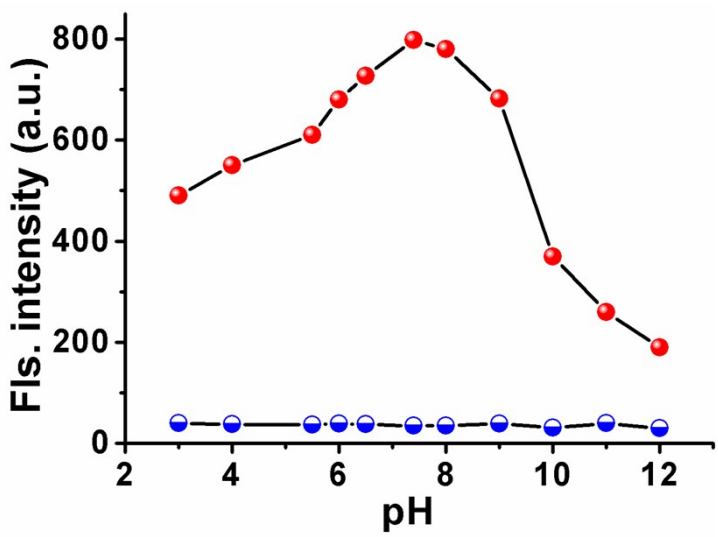

Fig. S7. pH effect on the fluorescence intensity of $\mathbf{H_3L}$ and $\mathbf{H_2L\text{-}Cu^{2+}}$ at λ = 425 nm (λ_{ex} = 365 nm) in DMF/0.02 M HEPES (1:1, v/v,) at different pH (*ca*. 3-12) medium.

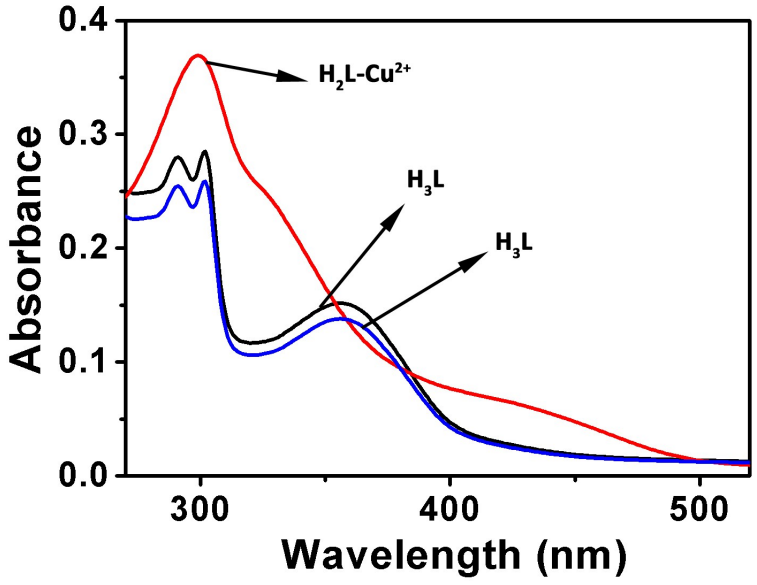

Fig. S8. UV-vis absorption spectra of $\mathbf{H_3L}$ and $\mathbf{H_2L\text{-}Cu^{2+}}$.

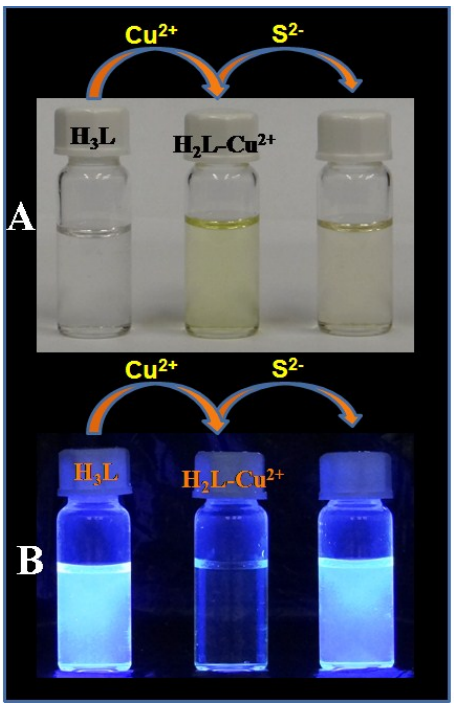

Fig. S9. Observed visual color changes in room light (A) and under UV (B) of probe **H_3L** upon addition of Cu^{2+} and S^{2-}, respectively, in DMF/0.02 M HEPES (1:1, v/v, pH = 7.4) medium.

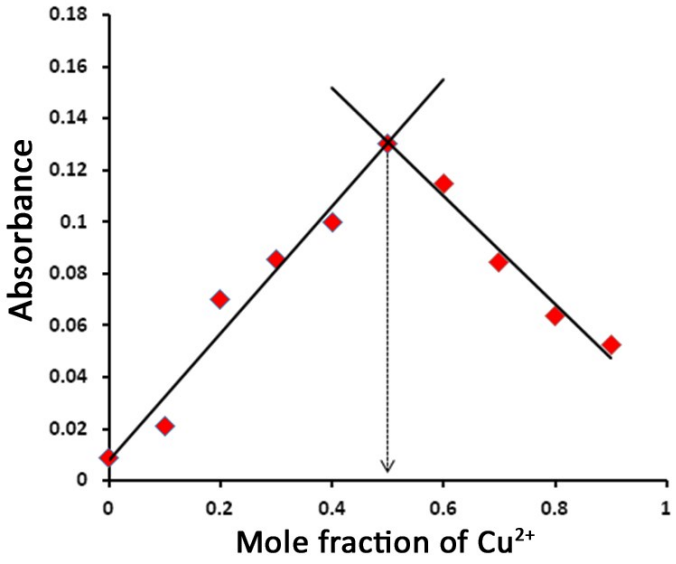

Fig. S10, Job's plot for **H_3L** and Cu^{2+} from absorption data at λ = 425 nm.

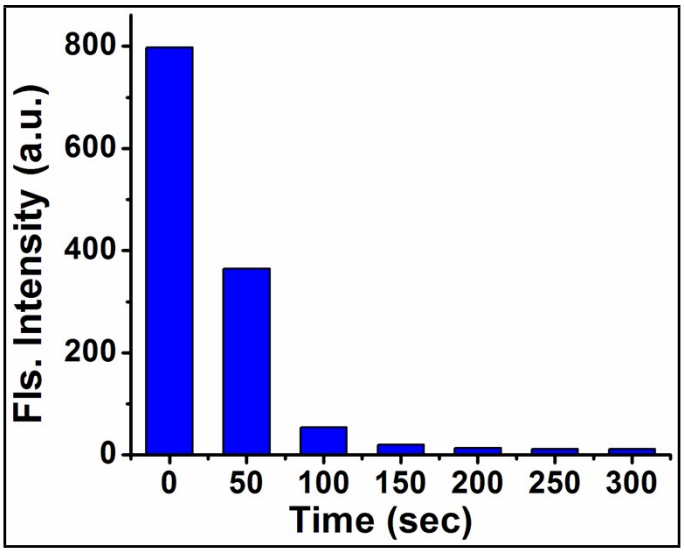

Fig. S11. Time dependent fluorescence response of $\mathbf{H_3L}$ at λ = 425 nm (λ_{ex} = 365 nm) (5 μM; DMF/0.02 M HEPES (1:1, v/v, pH = 7.4) in presence of *ca*. 5 equiv. of Cu^{2+} (5 μM).

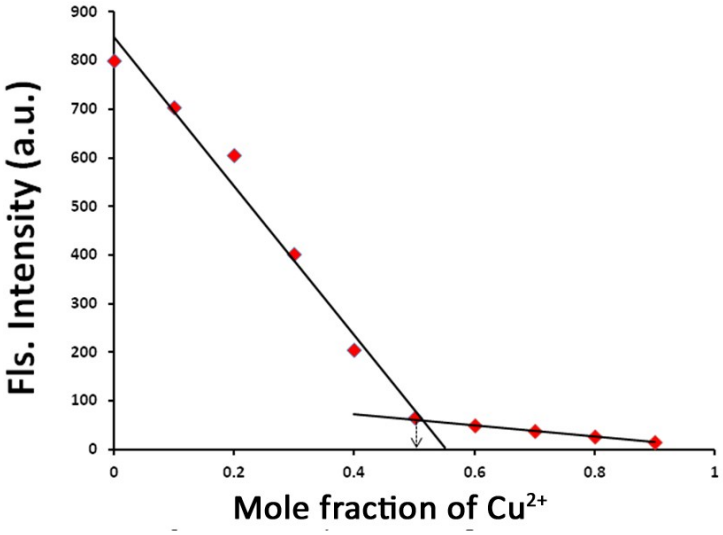

Fig. S12. Job's plot for the fluorescence titration of $\mathbf{H_3L}$ with Cu^{2+} ions at λ = 425 nm (λ_{ex} = 365 nm).

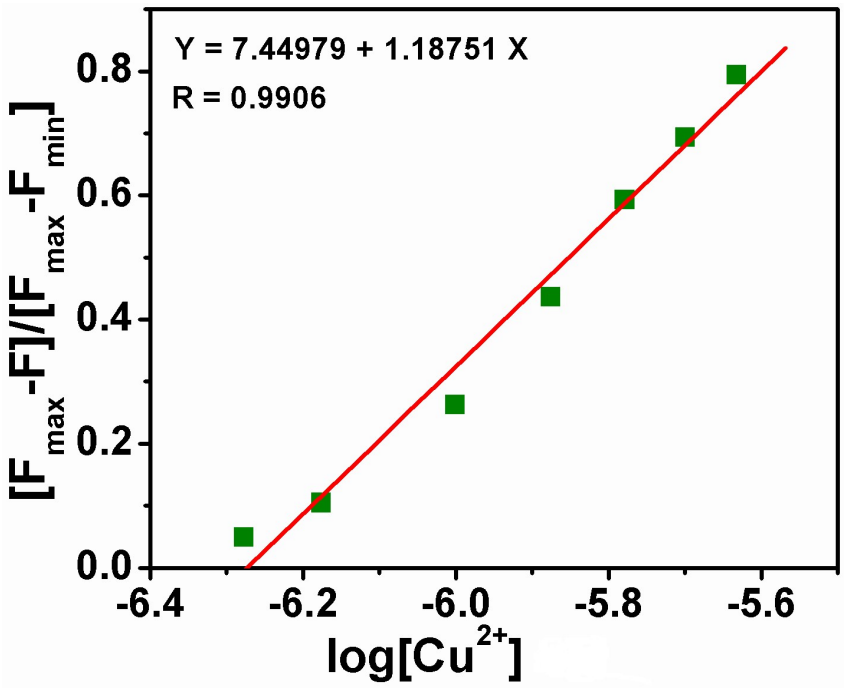

Fig. S13. Cu^{2+} ion detection limit plot for the sensor $\mathbf{H_3L}$. Concentration is in nM.

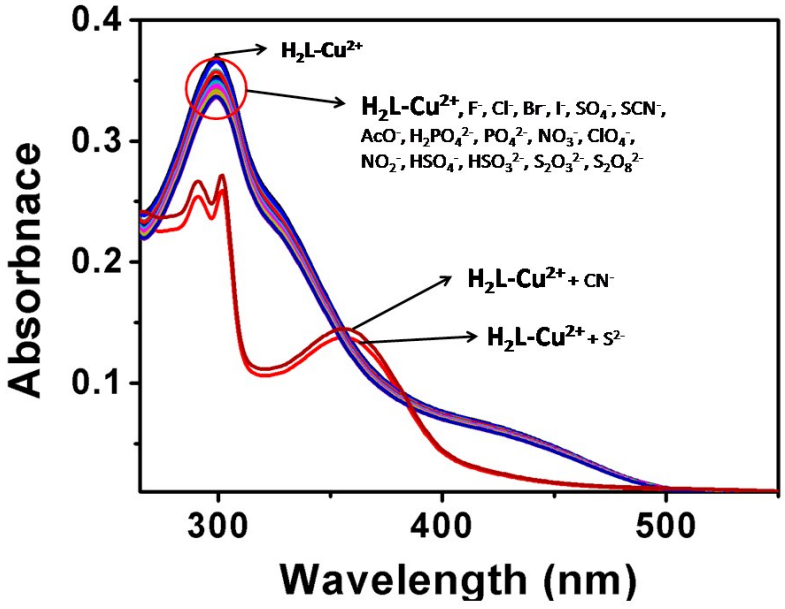

Fig. S14. Change in the absorbance of receptor $\mathbf{H_2L\text{-}Cu^{2+}}$ upon mixing with other anions.

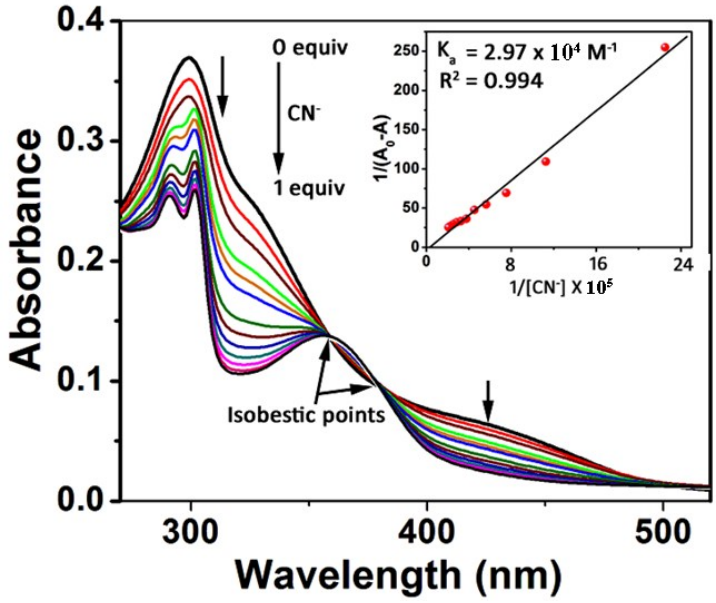

Fig. S15. Change in the absorption intensity of $\mathbf{H_2L\text{-}Cu^{2+}}$ (5 μM) upon gradual addition of CN^- solution in DMF/0.02 M HEPES (1:1, v/v, pH = 7.4) medium . Insets show the corresponding Benesi-Hildebrand plot.

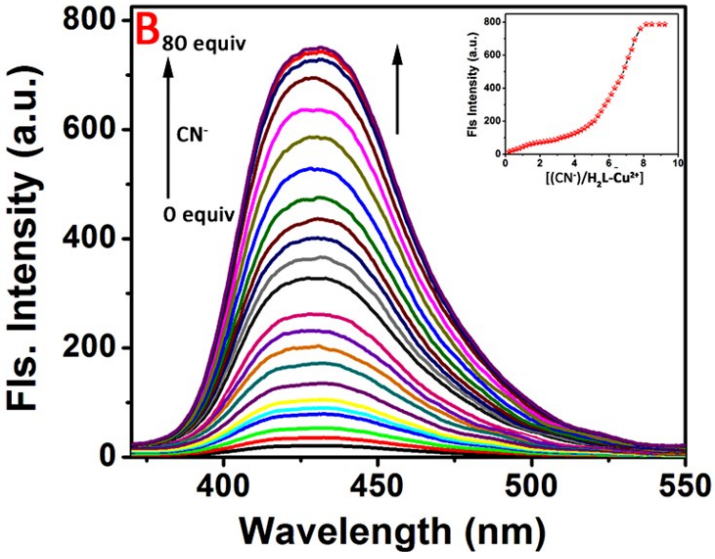

Fig. S16. Change in the fluorescence intensity of $\mathbf{H_2L\text{-}Cu^{2+}}$ (5 μM) upon gradual addition of CN^- solution in DMF/0.02 M HEPES (1:1, v/v, pH = 7.4) medium. Insets show the titration curve of $\mathbf{H_2L\text{-}Cu^{2+}}$ *vs*. the ratio of CN^- and $\mathbf{H_2L\text{-}Cu^{2+}}$ concentrations at λ = 425 nm (λ_{ex} = 365 nm).

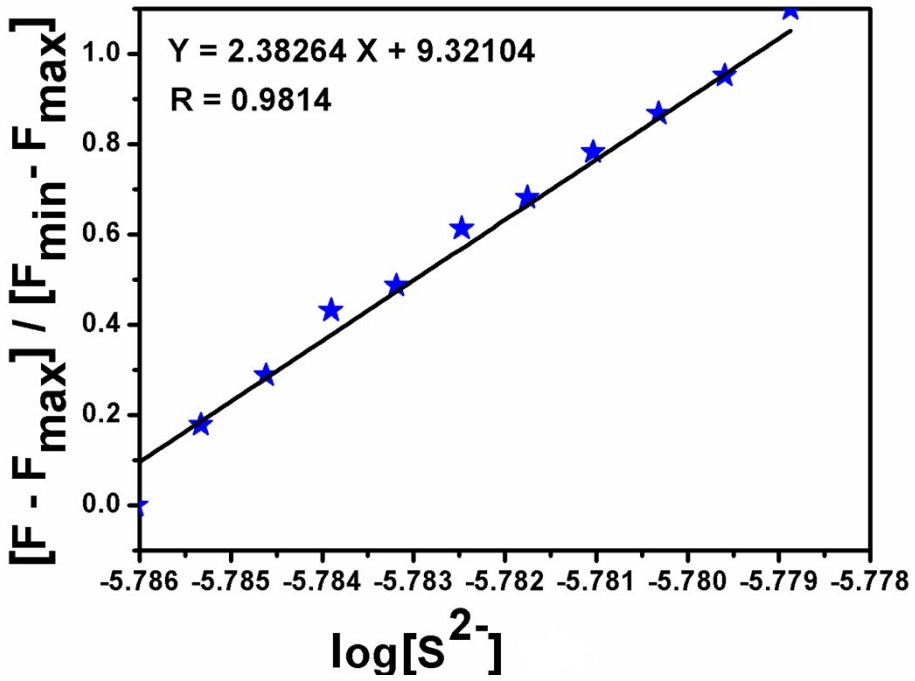

Fig. 17. S^{2-} ion detection limit plot for the sensor **H_2L-Cu^{2+}**. Concentration is in μM.

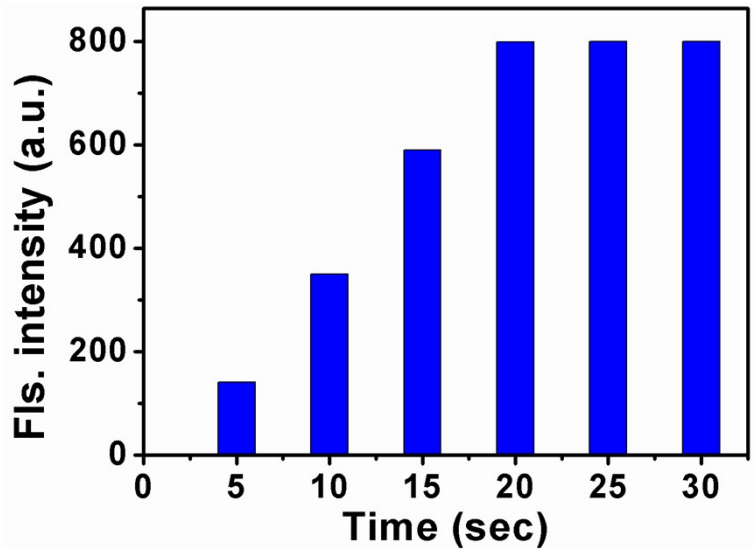

Fig. S18. Time dependent fluorescence response of **H_2L-Cu^{2+}** at λ = 425 nm (λ_{ex} = 365 nm) in DMF/0.02 M HEPES (1:1, v/v, pH = 7.4) medium in presence of *ca.* 3 equiv. of S^{2-}.

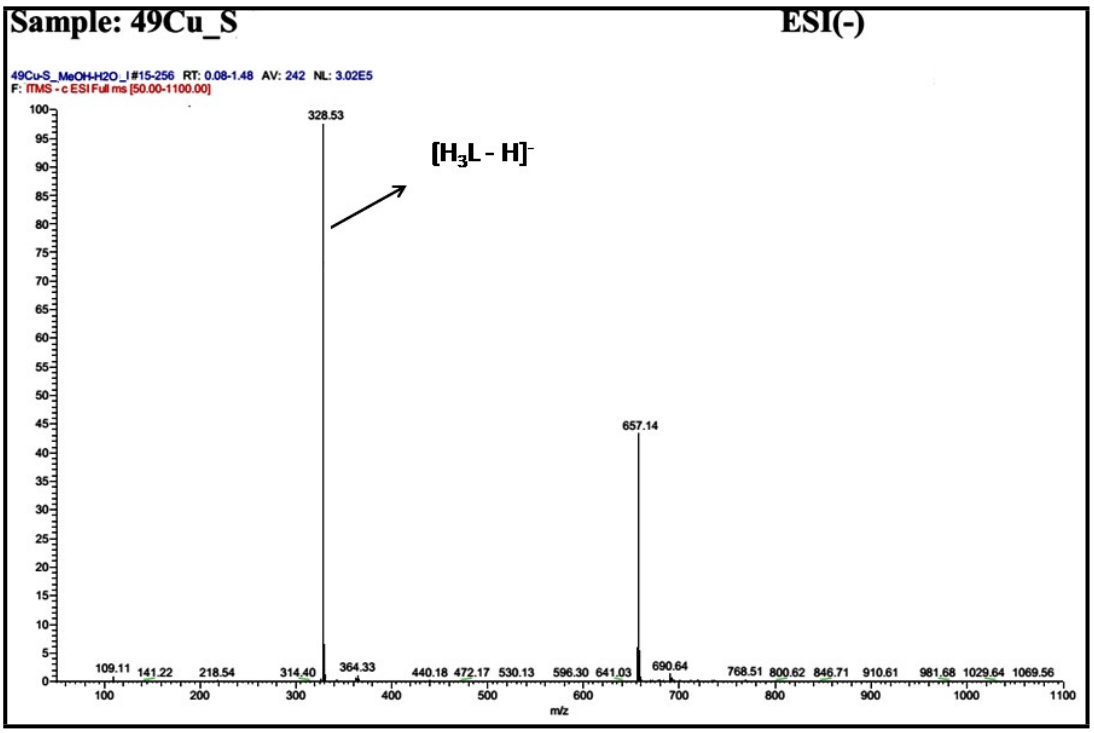

Fig. S19. ESI-MS spectrum of $\mathbf{H_2L\text{-}Cu^{2+}}$ in presence of 2 equiv. of Na_2S obtained in negative mode in methanol.

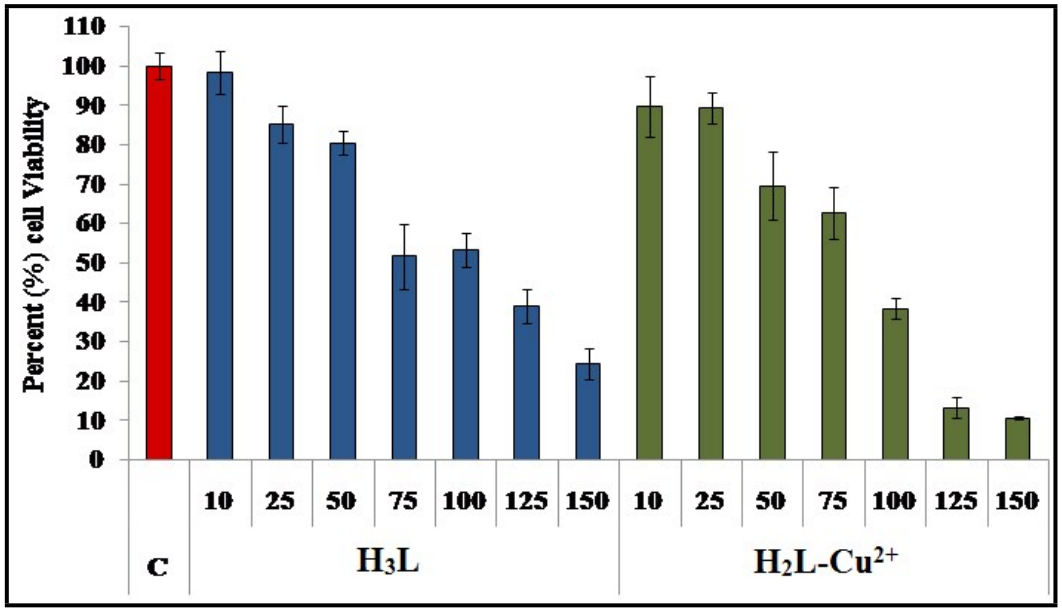

Fig. S20. Cytotoxicity and cell proliferation effect of $\mathbf{H_3L}$ and $\mathbf{H_2L\text{-}Cu^{2+}}$ were tested by MTT assay. DL cells were incubated with 10 to 150 μM concentrations of probes for 24 h.

References

1. Patiny, L.; Borel, A.; *Journal of Chemical Information and Modeling,* **2013.** http://www.chemcalc.org